

ENGR 580 Design Project Report

Dongming Wang

The University of British Columbia
Kelowna, BC, CA
dwang53@student.ubc.ca

Qingyu Wang

The University of British Columbia
Kelowna, BC, CA
qingyu.0126@gmail.com

I. INTRODUCTION

The flight of flying vehicle with fixed wing (most missiles and planes, etc.) is often affected by various disturbances from the external environment, such as changes in wind, airflow and other atmospheric conditions. These disturbances may cause the vehicle to deviate from its reference trajectory, thereby affecting its accuracy or hit rate. This project mainly focuses on modeling the lateral disturbance motion of the vehicle, and corrects various lateral disturbance motion parameters of the vehicle through the rudder deflection angle and aileron deflection angle.

A. Definition of Angles

- 1) Yaw angle ψ : The angle between the projection of the vehicle's longitudinal axis O_x on the horizontal plane and the A_x axis of the ground coordinate system.
- 2) Roll angle γ : The angle between the vehicle's O_y axis and the vertical plane containing the vehicle's longitudinal axis O_x . As shown in figure 1 and 2.
- 3) ballistic deflection angle ψ_v : The angle between the projection of the vehicle's velocity vector on the horizontal plane and the A_x axis of the ground coordinate system.
- 4) sideslip angle β : The angle between the velocity vector and the longitudinal plane of symmetry [1], [2]. The relation between ψ , ψ_v and β can be shown in figure 3.

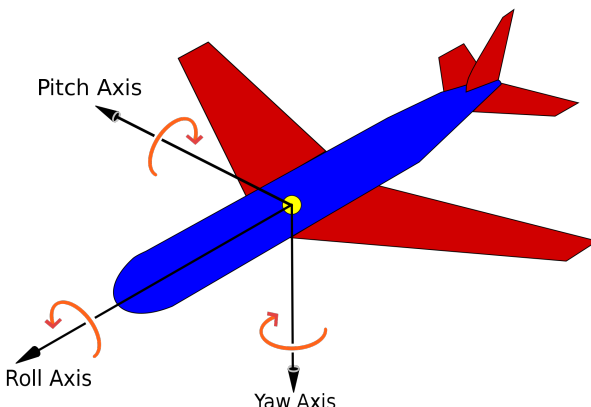


Fig. 1. The angles of rotation in three dimensions

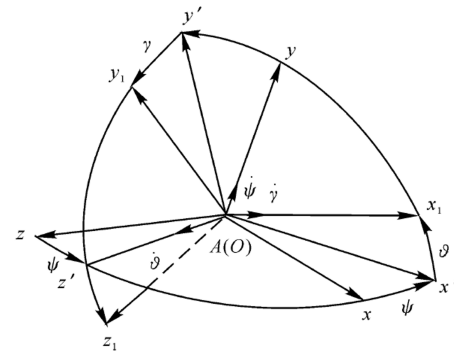


Fig. 2. From Earth frame to body frame

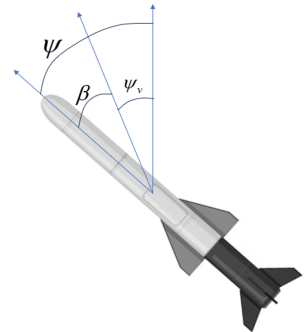


Fig. 3. The relation between ψ , ψ_v and β

B. Functional Explanation

In real vehicle flights, deviations from the ideal trajectory always occur due to various reasons, primarily attributed to additional aerodynamic forces and moments acting on the missile. This project aims to model the discrepancies between the actual and ideal values of various flight parameters (referred to as disturbances) during the flight process. By manipulating the control surfaces, namely the vehicle's rudders, the deviations are minimized to zero, thereby eliminating any disturbances present during the flight process. The objective is to achieve the elimination of disturbances in any flight scenario by adjusting the control mechanisms to counteract the deviations from the ideal trajectory.

C. Major Assumptions

- 1) The lateral motion parameters β , γ , γ_v , ψ , ψ_v , ω_x , ω_y , and z are all small quantities, so

$\cos \beta = \cos \gamma = \cos \gamma_v \approx 1$, and the influence of the product of each small quantity such as $\sin \beta \sin \gamma$, $\omega_y \sin \gamma$, $\omega_x \omega_y$ can be omitted (This assumption will be used a lot in the following linearization).

- 2) The vehicle basically flies in a certain vertical plane, that is, its actual 3D flight trajectory is not much different from the trajectory in the 2D vertical plane.

Justification: Since this project is about the lateral disturbance elimination, the model will mostly focus on the lateral motion of a vehicle. This assumption is used to simplify the model. Moreover, in the actual flight, there are many angles coupled with angles in the other directions, thus causes the difficulties in decoupling and the model building. To simplify this model and calculation, this assumption is made.

- 3) The deflection of the pitch control mechanism only depends on the longitudinal motion parameters, while the deflection of the yaw and roll control mechanisms only depends on the lateral motion parameters.

Justification: This assumption is made for further decoupling.

- 4) The aircraft is a normal layout aircraft, and the impact of the downwash delay of the front-end mechanism on the lift mechanism is not considered.

Justification: The aerodynamic performance of an aircraft largely depends on its layout. Two common layouts are normal layout with its rudder behind the wing and Canard layout with its rudders in front of the wing. As shown in figure 4 and 5.

Also, a phenomenon called ‘Downwash delay’ would happen if a flow passes an airfoil and generates a vortex on its tip, causes pressure change on the lifting actuator after that, which can be shown in 6.

Normally, when calculating the force coefficient and torque coefficient for a canard aircraft, this downwash delay cannot be neglected, and it is comparably difficult to calculate or measure. Therefore, this assumption is made.

- 5) The aircraft control system has no errors, and the actuator (rudder surface) can respond accurately according to instructions.

Justification: This assumption is made to model the ideal scenario, eliminate the unnecessary errors.



Fig. 4. Normal layout in MiG-25 [3]



Fig. 5. Canard layout in J-20 [4]

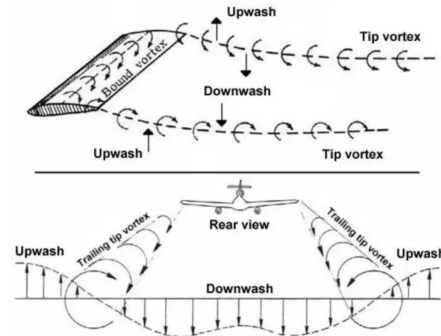


Fig. 6. Downwash delay [5]

II. DESCRIPTION OF THE SYSTEM

A. States Definition

The states of the system are defined as x [1], [2]:

$$\mathbf{x} = \begin{bmatrix} \omega_x \\ \omega_y \\ \beta \\ \gamma \end{bmatrix}$$

- ω_x Rotational angular velocity along the x-axis;
- ω_y Rotational angular velocity along the y-axis;
- β Sideslip angle;
- γ Roll angle.

All these states are lateral perturbation motion parameters.

B. Input Definition

The inputs of the system are defined as u [1], [2]:

$$\mathbf{u} = \begin{bmatrix} \delta_x \\ \delta_y \end{bmatrix}$$

δ_x Rudder deflection angle along the x-axis;
 δ_y Rudder deflection angle along the y-axis.

C. Output Definition

The outputs of the system are defined as $y = x$ [1], [2]:

$$\mathbf{y} = \begin{bmatrix} \omega_x \\ \omega_y \\ \beta \\ \gamma \end{bmatrix}$$

D. Nonlinear System Representation

1) *Original Nonlinear Equation:* The original nonlinear lateral equation is [1], [2]:

$$\left\{ \begin{array}{l} \dot{\psi}_v = \frac{P(\sin \alpha \sin \gamma_v - \cos \alpha \sin \beta \cos \gamma_v)}{-mv \cos \theta} + \frac{Y \sin \gamma_v + Z \cos \gamma_v}{-mv \cos \theta} \\ \dot{\omega}_x = \frac{M_x}{J_x} - \frac{(J_z - J_y)\omega_y \omega_z}{J_x} \\ \dot{\omega}_y = \frac{M_y}{J_y} - \frac{(J_x - J_z)\omega_z \omega_x}{J_y} \\ \dot{\psi} = \frac{\omega_y \cos \gamma - \omega_z \sin \gamma}{\cos \vartheta} \\ \dot{\gamma} = \omega_x - \tan \vartheta (\omega_y \cos \gamma - \omega_z \sin \gamma) \\ \dot{z} = -v \cos \theta \sin \psi_v \\ \sin \psi_v \cos \theta = \cos \alpha \cos \beta \sin \psi \cos \vartheta \\ \quad + \sin \alpha \cos \beta \sin \gamma \cos \psi \\ \quad + \sin \alpha \cos \beta \cos \gamma \sin \psi \sin \vartheta \\ \quad - \sin \beta \cos \gamma \cos \psi \\ \quad + \sin \beta \sin \gamma \sin \psi \sin \vartheta \\ \sin \gamma_v \cos \theta = \cos \alpha \sin \beta \sin \vartheta \\ \quad - \sin \alpha \sin \beta \cos \gamma \cos \vartheta \\ \quad + \cos \beta \sin \gamma \cos \vartheta \end{array} \right.$$

where:

$$\left\{ \begin{array}{l} M_x = M_x^{\omega_x} \omega_x + M_x^{\omega_y} \omega_y + M_x^\beta \beta + M_x^{\delta_x} \delta_x + M_x^{\delta_y} \delta_y \\ M_y = M_y^{\omega_x} \omega_x + M_y^{\omega_y} \omega_y + M_y^\beta \beta + M_y^{\dot{\beta}} \dot{\beta} + M_y^{\delta_y} \delta_y \end{array} \right.$$

2) *Simplified Nonlinear Equation:* The original equation can be transformed and simplified as:

$$\left\{ \begin{array}{l} \dot{\omega}_x = \frac{M_x^{\omega_x}}{J_x} \omega_x + \frac{M_x^{\omega_y}}{J_x} \omega_y + \frac{M_x^\beta}{J_x} \beta + \frac{M_x^{\delta_x}}{J_x} \delta_x + \frac{M_x^{\delta_y}}{J_x} \delta_y \\ \dot{\omega}_y = \frac{M_y^{\omega_x}}{J_y} \omega_x + \frac{M_y^{\omega_y}}{J_y} \omega_y + \frac{M_y^\beta}{J_y} \beta + \frac{M_y^{\dot{\beta}}}{J_y} \dot{\beta} + \frac{M_y^{\delta_y}}{J_y} \delta_y \\ \dot{\beta} = \frac{\cos \theta (\cos \gamma - \omega_z \sin \gamma)}{\cos \vartheta} \omega_y - \frac{P - Z^\beta}{mv} \beta \\ \quad + \frac{g}{v} \cos \alpha \sin \beta \sin \vartheta \\ \quad - \frac{g}{v} \sin \alpha \sin \beta \cos \gamma \cos \vartheta \\ \quad + \frac{g}{v} \cos \beta \sin \gamma \cos \vartheta \\ \quad + \frac{Z^{\delta_y}}{mv} \delta_y + \alpha \dot{\gamma} \\ \dot{\gamma} = \omega_x - \tan \vartheta (\omega_y \cos \gamma - \omega_z \sin \gamma) \end{array} \right.$$

The nomenclature for the equations will be presented in section II-E3.

E. Local Linearization

1) *Linearized Equation:* We assume the equilibrium point is at $\mathbf{x} = [0, 0, 0, 0]^T$ and $\mathbf{u} = [0, 0]^T$. After linearization, the equation can be written as:

$$\left\{ \begin{array}{l} \Delta \dot{\psi}_v = \frac{P - Z^\beta}{mv \cos \theta} \Delta \beta - \frac{P \alpha + Y}{mv \cos \theta} \Delta \gamma_v \\ \quad - \frac{Z^{\delta_y}}{mv \cos \theta} \Delta \delta_y \\ \Delta \dot{\omega}_x = \frac{M_x^{\omega_x}}{J_x} \Delta \omega_x + \frac{M_x^{\omega_y}}{J_x} \Delta \omega_y \\ \quad + \frac{M_x^\beta}{J_x} \Delta \beta + \frac{M_x^{\delta_x}}{J_x} \Delta \delta_x + \frac{M_x^{\delta_y}}{J_x} \Delta \delta_y \\ \Delta \dot{\omega}_y = \frac{M_y^{\omega_x}}{J_y} \Delta \omega_x + \frac{M_y^{\omega_y}}{J_y} \Delta \omega_y \\ \quad + \frac{M_y^\beta}{J_y} \Delta \beta + \frac{M_y^{\dot{\beta}}}{J_y} \Delta \dot{\beta} + \frac{M_y^{\delta_y}}{J_y} \Delta \delta_y \\ \Delta \dot{\psi} = \frac{1}{\cos \vartheta} \Delta \omega_y \\ \Delta \dot{\gamma} = \Delta \omega_x - \tan \vartheta \Delta \omega_y \\ \Delta \dot{z} = -v \cos \theta \Delta \psi_v \\ \Delta \psi_v = \Delta \psi + \frac{\alpha}{\cos \theta} \Delta \gamma - \frac{1}{\cos \theta} \Delta \beta \\ \Delta \gamma_v = \tan \theta \Delta \beta + \frac{\cos \vartheta}{\cos \theta} \Delta \gamma \end{array} \right.$$

2) *Simplified Linearized Equation:* Because all the parameters can be represented by the following independent

parameters: $\Delta\omega_x$, $\Delta\omega_y$, $\Delta\beta$, $\Delta\gamma$ [1], [2]. The equation can be simplified as:

$$\left\{ \begin{array}{l} \Delta\dot{\omega}_x = \frac{M_x^{\omega_x}}{J_x}\Delta\omega_x + \frac{M_x^{\omega_y}}{J_x}\Delta\omega_y \\ \quad + \frac{M_x^\beta}{J_x}\Delta\beta + \frac{M_x^{\delta_x}}{J_x}\Delta\delta_x + \frac{M_x^{\delta_y}}{J_x}\Delta\delta_y \\ \Delta\dot{\omega}_y = \frac{M_y^{\omega_x}}{J_y}\Delta\omega_x + \frac{M_y^{\omega_y}}{J_y}\Delta\omega_y \\ \quad + \frac{M_y^\beta}{J_y}\Delta\beta + \frac{M_y^{\dot{\beta}}}{J_y}\Delta\dot{\beta} + \frac{M_y^{\delta_y}}{J_y}\Delta\delta_y \\ \cos\theta\Delta\dot{\psi}_v = \frac{\cos\theta}{\cos\vartheta}\Delta\omega_y + \alpha\Delta\dot{\gamma} - \Delta\dot{\beta} \\ \quad = \frac{P - Z^\beta}{mv}\Delta\beta - \frac{Z^{\delta_y}}{mv}\Delta\delta_y \\ \quad - \left(\frac{g}{v}\sin\theta\right)\Delta\beta - \left(\frac{g}{v}\cos\vartheta\right)\Delta\gamma \\ \Delta\dot{\gamma} = \Delta\omega_x - \tan\vartheta\Delta\omega_y \end{array} \right.$$

3) *Notations for the simplified equations and realistic numerical values:* The definition of the parameters is shown in table I. In this project, the parameters from MIM-104 Patriot missile [6], [7] are used to calculate the dynamic coefficients at the equilibrium point, as shown in table II. By defining the dynamics coefficients as follows, and substituting the parameters above in the equations, the dynamic coefficients is shown in table III.

4) *Final Linearized Equation:*

$$\left\{ \begin{array}{l} \Delta\dot{\omega}_x = -b_{11}\Delta\omega_x - b_{12}\Delta\omega_y - b_{14}\Delta\beta \\ \quad - b_{18}\Delta\delta_x - b_{17}\Delta\delta_y \\ \Delta\dot{\omega}_y = -b_{21}\Delta\omega_x - b_{22}\Delta\omega_y - b_{24}\Delta\beta \\ \quad - b_{24}\Delta\dot{\beta} - b_{27}\Delta\delta_y \\ \Delta\dot{\beta} = -b_{32}\Delta\omega_y - (b_{34} + a_{33})\Delta\beta \\ \quad + \alpha\Delta\dot{\gamma} - b_{35}\Delta\gamma - b_{37}\Delta\delta_y \\ \Delta\dot{\gamma} = \Delta\omega_x + b_{52}\Delta\omega_y \end{array} \right.$$

5) *State Space Function:* The state space function can be written as:

$$\left\{ \begin{array}{l} \dot{x} = Ax + Bu \\ y = Cx + Du \end{array} \right.$$

$$\left\{ \begin{array}{l} A = \begin{bmatrix} -b_{11} & -b_{12} & -b_{14} & 0 \\ A_{21} & A_{22} & A_{23} & A_{24} \\ \alpha & A_{32} & A_{33} & -b_{35} \\ 1 & b_{52} & 0 & 0 \end{bmatrix} \\ B = \begin{bmatrix} -b_{18} & -b_{17} \\ 0 & -b_{27} + b_{24}b_{37} \\ 0 & -b_{37} \\ 0 & 0 \end{bmatrix} \\ C = \begin{bmatrix} 1 & 0 & 0 & 0 \\ 0 & 1 & 0 & 0 \\ 0 & 0 & 1 & 0 \\ 0 & 0 & 0 & 1 \end{bmatrix} \\ D = \begin{bmatrix} 0 & 0 \\ 0 & 0 \\ 0 & 0 \\ 0 & 0 \end{bmatrix} \end{array} \right.$$

$$\left\{ \begin{array}{l} A_{21} = -b_{21} - \dot{b}_{24}\alpha \\ A_{22} = -b_{22} + \dot{b}_{24}b_{32} - \dot{b}_{24}b_{52}\alpha \\ A_{23} = -b_{24} + \dot{b}_{24}b_{34} - \dot{b}_{24}a_{33} \\ A_{24} = +\dot{b}_{24}b_{35} \\ A_{32} = -b_{32} + b_{52}\alpha \\ A_{33} = -b_{34} - a_{33} \end{array} \right.$$

When we put the real value in to the formula, we will get:

$$\left\{ \begin{array}{l} A = \begin{bmatrix} -1.8600 & -0.6600 & -8.8000 & 0 \\ -0.0200 & -0.2000 & -3.0000 & 0 \\ 0.2618 & 0.9991 & -0.0600 & 0.0280 \\ 1.0000 & -0.0034 & 0 & 0 \end{bmatrix} \\ B = \begin{bmatrix} -0.9800 & -0.7800 \\ 0 & -0.9000 \\ 0 & -0.0180 \\ 0 & 0 \end{bmatrix} \\ C = \begin{bmatrix} 1 & 0 & 0 & 0 \\ 0 & 1 & 0 & 0 \\ 0 & 0 & 1 & 0 \\ 0 & 0 & 0 & 1 \end{bmatrix} \\ D = \begin{bmatrix} 0 & 0 \\ 0 & 0 \\ 0 & 0 \\ 0 & 0 \end{bmatrix} \end{array} \right.$$

III. LIMITATION

- Due to assumption 2, the motion mode in the lateral plane of the aircraft is relatively simple, so as to decouple the

longitudinal perturbation motion and the lateral perturbation motion of the aircraft. However, during the actual flight of an aircraft, especially during the mission of a long-range rocket or ballistic vehicle, the lateral movement of the aircraft will also be very complicated due to the influence of factors such as the shape of the earth and the Coriolis force. The corresponding decoupling of the two motion modes will be more difficult.

- In the process of simulation testing with given actual values, many parameters of this project cannot find their reference sources and require manual estimation. In actual situations, most dynamic coefficients are measured experimentally rather than calculated.

IV. HANDOUT 2

A. Handout 2 - Question 3.1

The system has 2 inputs, 4 states, 4 outputs.

B. Handout 2 - Question 3.2

The Jordan Normal Form and eigenvalues of our linearized system is:

$$J = \begin{bmatrix} \lambda_1 & 0 & 0 & 0 \\ 0 & \lambda_2 & 0 & 0 \\ 0 & 0 & \lambda_3 & 0 \\ 0 & 0 & 0 & \lambda_4 \end{bmatrix}$$

$$\left\{ \begin{array}{l} \lambda_1 = -1.2003 \\ \lambda_2 = +0.0011 \\ \lambda_3 = -0.4604 - 2.1148i \\ \lambda_4 = -0.4604 + 2.1148i \end{array} \right.$$

Both algebraic and geometric multiplicity of each eigenvalue is 1.

C. Handout 2 - Question 3.3

Because not all the eigenvalues of our system have negative real parts, our linearized system is unstable.

D. Handout 2 - Question 3.4

Because our linearized system is unstable, our nonlinear system is also locally unstable at the equilibrium point.

E. Handout 2 - Question 3.5

The poles of each entries of the transfer function is:

$$\left\{ \begin{array}{l} pole_1 = -1.2003 \\ pole_2 = +0.0011 \\ pole_3 = -0.4604 - 2.1148i \\ pole_4 = -0.4604 + 2.1148i \end{array} \right.$$

So our linearized system is not BIBO stable.

F. Handout 2 - Question 3.6

The experiment can not be conducted since the cost is too high.

G. Handout 2 - Question 3.7

The homogeneous response simulations last for 1000s, with the initial condition being as:

$$\mathbf{x}_0 = \begin{bmatrix} 0.1 \\ 0.1 \\ 0.05 \\ 0.05 \end{bmatrix}$$

which means the aircraft is suffered from a disturbance that caused the aircraft's yaw angle and roll angle to deviate by 0.05 degrees each.

The homogeneous response of the linear and nonlinear system can be illustrated as below:

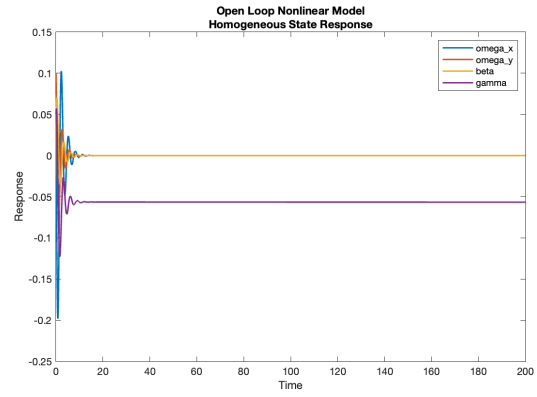


Fig. 7. Homogeneous response of nonlinear system

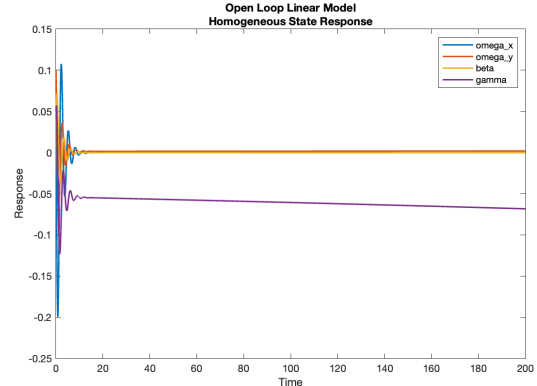


Fig. 8. Homogeneous response of linear system

It can be seen from fig. 7 and 8 that the yaw angles of linear and nonlinear systems are different, with it in linear system demonstrating an unstable trend and the other a stable trend, which are consistent with the characteristics of the previously calculated eigenvalues. This can be attributed to the assumptions and approximations that are applied in linearizing the model that introduces the system errors. Since in the approximations, the yaw angle is approximated from $\sin\gamma$ to only γ , and as gamma grows, the approximation will gradually introduce error to the system as it no longer stands, leading to the result of fig. 8.

H. Handout 2 - Question 3.8

The forced response of both linear and nonlinear system are simulated with step changes of 0.01 in each input. This value is within the rudder deflection angle adjustment range of most aircraft, which means the step input can be performed on the real system easily. And it's small enough to simulate the conditions of small disturbances encountered by the aircraft during flight.

$$\begin{aligned}\delta_x &= 0.01 \\ \delta_y &= 0.01\end{aligned}$$

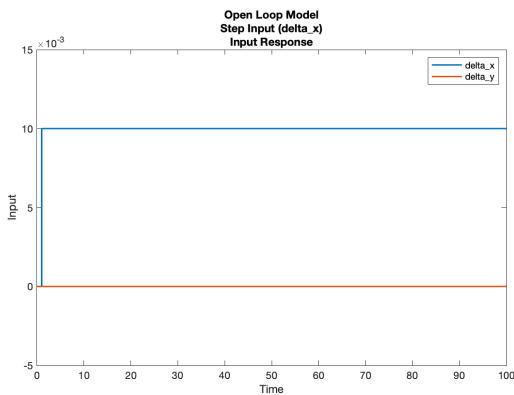


Fig. 9. Forced input for δ_y

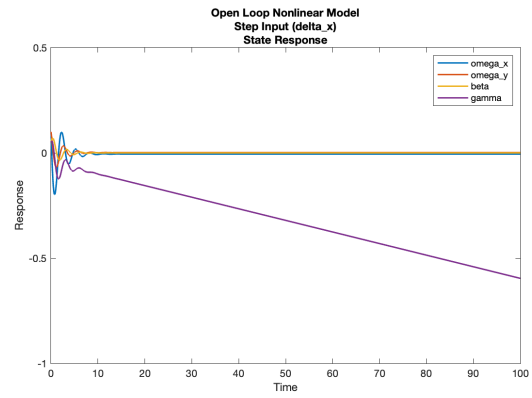


Fig. 11. Forced response of nonlinear system for step input δ_x

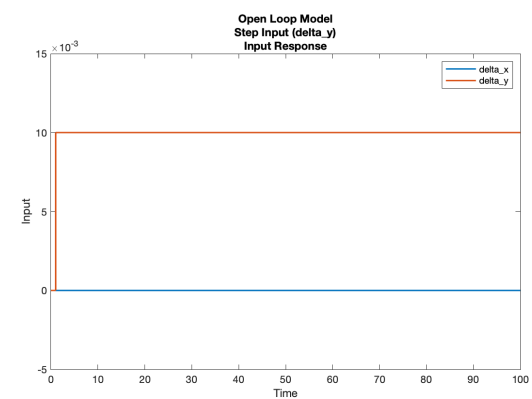


Fig. 12. Forced input for δ_y

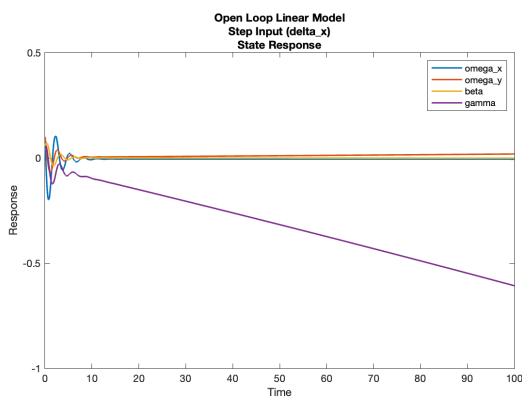


Fig. 10. Forced response of linear system for step input δ_x

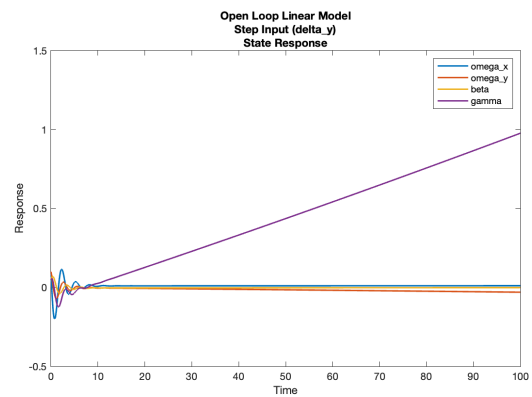


Fig. 13. Forced response of linear system for step input δ_y

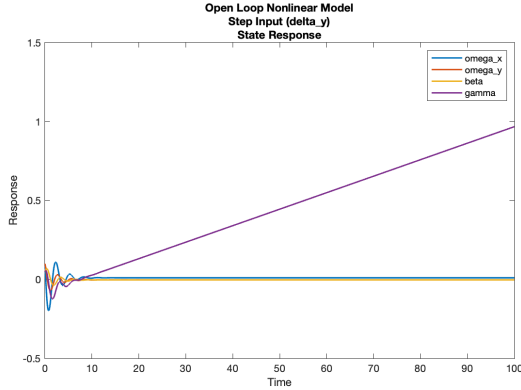


Fig. 14. Forced response of nonlinear system for step input δ_y

I. Handout 2 - Question 3.9

As shown in Fig.9, by assigning δ_x of 0.01, the general trend of linear system response and nonlinear system response is shown in Fig.10 and Fig.11, which is basically the same, with γ , the yaw angle, being unstable as simulation time goes. And this BIBO result still matches the poles that is calculated before. But the finite values of the other three states in the nonlinear system demonstrates a much better stability than them in linear model, which can also be attributed to the assumptions and approximations that are applied in linearizing the model. The similar trend can be found in the $\delta_y = 0.01$ case, as shown in Fig.12, Fig.13 and Fig.14. One interesting fact is that in the real aircraft motion, this instability in the roll angle is sometimes reasonable, and this instability is named 'Dutch Roll', which will take place when the lateral stability is better than the rolling stability of the aircraft. And the aircraft will be in spiral motion when certain conditions are triggered.

J. Handout 2 - Question 3.10

There's many criterion to judge a aircraft according to its application, since project is based on the MIM-104 Patriot missile, the maneuverability is of great concern. According to the MIM-104 specification table [7], the missile overload range is 25-30g, that means the acceleration required for the missile's angular velocity to return to zero within a specific period of time needs to be less than 30g. Since the M1M104 missile is a ground-to-air missile and its main target is missiles or fighter aircraft, it needs to make highly maneuverable actions in a short time to respond to the target's maneuvers. This project sets the response time to a maximum of 1s. The the minimum angular velocity, which is the specification requirement for overshoot of state 1 and 2 can be obtained from:

$$\begin{aligned}\omega_{\min} &= \text{Overload} \cdot L \cdot \text{time} \\ &= 25 \times 9.81 \times 1 \times 5.31 = 1302.2775 \text{ rad/s}\end{aligned}$$

V. HANDOUT 3

A. Handout 3 - Question 2.1

The controllability matrix of our system is:

$$\mathcal{C} = \begin{bmatrix} -0.9800 & 0 & 0 & 0 \\ -0.7800 & -0.9000 & -0.0180 & 0 \\ 1.8228 & 0.0196 & -0.2566 & -0.9800 \\ 2.2033 & 0.2496 & -1.1023 & -0.7770 \\ -1.1456 & 0.7293 & 0.4848 & 1.8228 \\ 5.4377 & 3.2131 & 0.8706 & 2.2025 \\ -2.6163 & -1.5772 & 0.4507 & -1.1481 \\ -19.8964 & -3.3633 & 4.6432 & 5.4269 \end{bmatrix}^T$$

The rank of the controllability matrix is 4, which is full rank, so the system is controllable.

B. Handout 3 - Question 2.2

Since our system is controllable, we don't need to calculate the controllable decomposition, and our system is stabilizable.

C. Handout 3 - Question 2.3

According to the attached m file, this system is controllable no matter which actuator fails.

D. Handout 3 - Question 2.4

As written in IV-J, there's specification for the response time as well as the overshoot of angular velocity. Moreover, in terms of the input, there's a rudder angle range for this missile. All the specifications can be shown as:

$$\begin{cases} \sigma_{x_1} < 1302.2775 \text{ rad/s} \\ \sigma_{x_2} < 1302.2775 \text{ rad/s} \\ -30^\circ < \delta_x < 30^\circ \\ -30^\circ < \delta_y < 30^\circ \\ t_{\text{response}} < 1 \text{ s} \end{cases}$$

E. Handout 3 - Question 2.5

All three methods are coded in the attached m file. After tuning, it was found that the system's angular velocity requirements are easily met. Generally, the magnitude of the angular velocity overshoot will be less than 10° , which is far smaller than the calculated angular velocity extreme value. We have only defined the requirements for two of the four states, so the four states have different weights, so LQR is more suitable for tuning this system. The figures below shows the status response and input of linear and nonlinear with LQR controller.

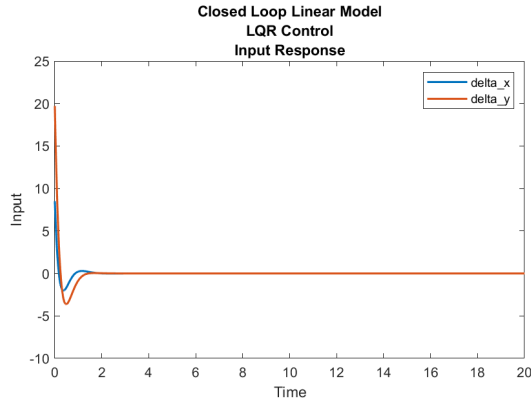


Fig. 15. Input response of closed loop linear system with LQR controller

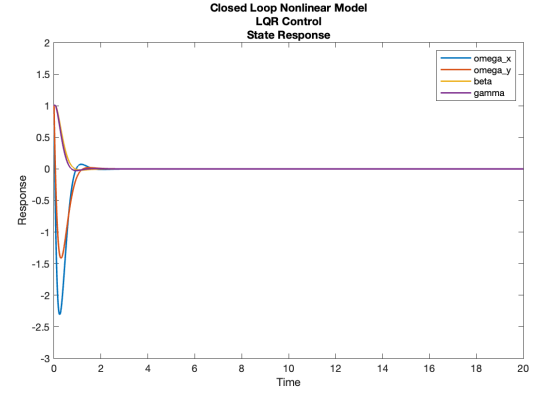


Fig. 18. States response of closed loop nonlinear system with LQR controller

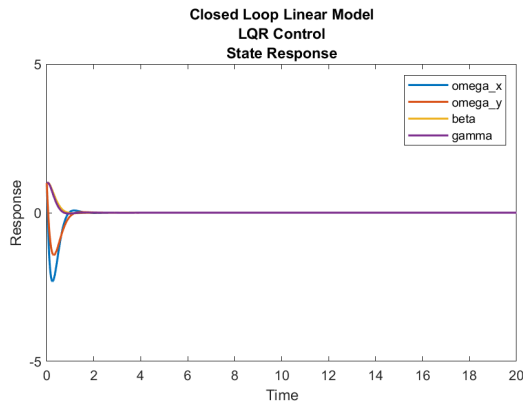


Fig. 16. States response of closed loop linear system with LQR controller

One thing interesting we found when tuning LQR is that when we try to increase the weights for the first two states, which is ω_x and ω_y , to meet the time requirement, the other two states will never meet the time requirement at the same time, and their response time are getting even longer. This is because the derivatives of the last two states are components of the first two states, and when the first two states converge fast, the last two will correspondingly converge slow. And the right way to tune the LQR is actually not increasing the weight of the first two state, but increasing the weight of the last two. And by doing this the response time of the first two will automatically become smaller.

F. Handout 3 - Question 2.6

The response to the initial condition of $x(t = 0) = 5x_0$ are:

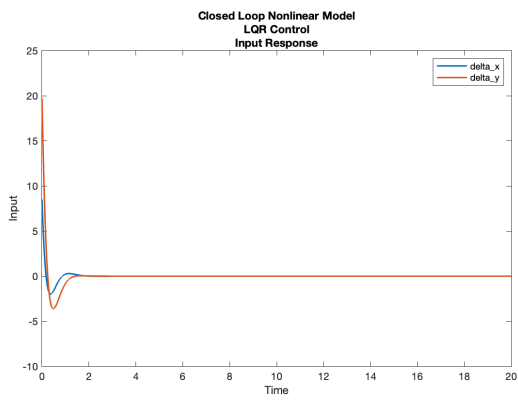


Fig. 17. Input response of closed loop nonlinear system with LQR controller

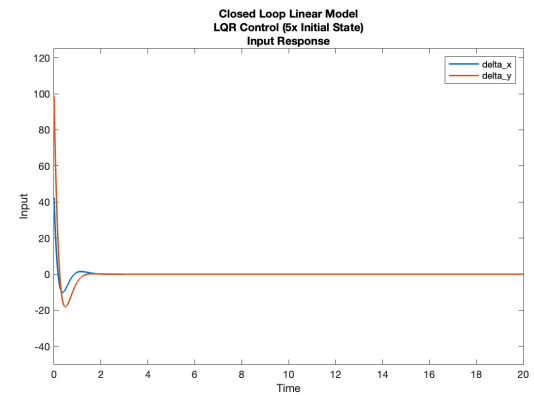


Fig. 19. Input response of closed loop linear system with LQR controller and $5x_0$

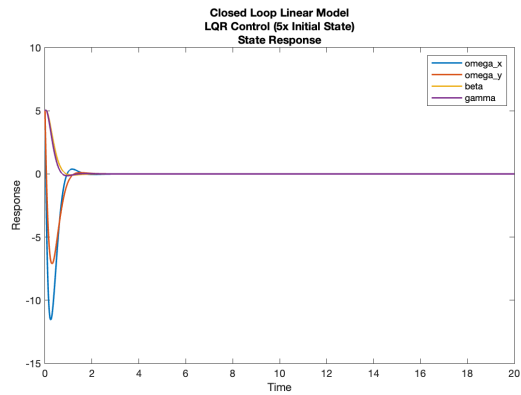


Fig. 20. States response of closed loop linear system with LQR controller and $5x_0$

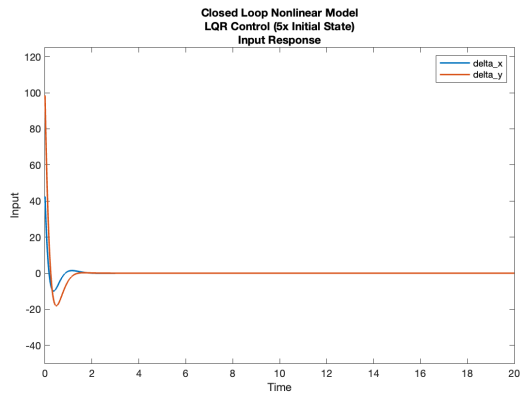


Fig. 21. Input response of closed loop nonlinear system with LQR controller and $5x_0$

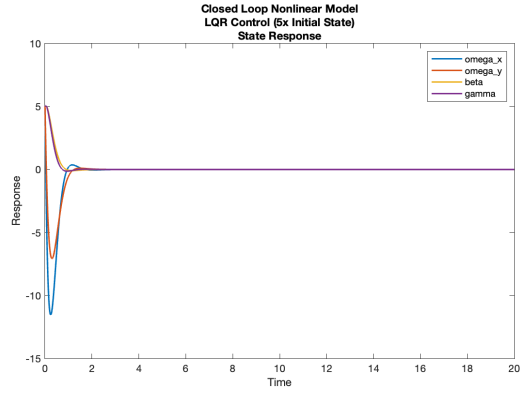


Fig. 22. States response of closed loop nonlinear system with LQR controller and $5x_0$

It can be seen from the comparison of the fig. 15-18 and fig. 19-22 that even if the initial state is changed to five times the original state, the tuned LQR controller still shows good control effects, and the parameters of each state still meet the requirements. However, the input value also becomes five times

the original value, causing part of the input curve to fail to fall within its value range.

G. Handout 3 - Question 2.7

In SIMULINK, we add noise of 0.0000, 0.0001, 0.0010, 0.0100 to the linear and nonlinear closed-loop models respectively and evaluate the homogeneous response.

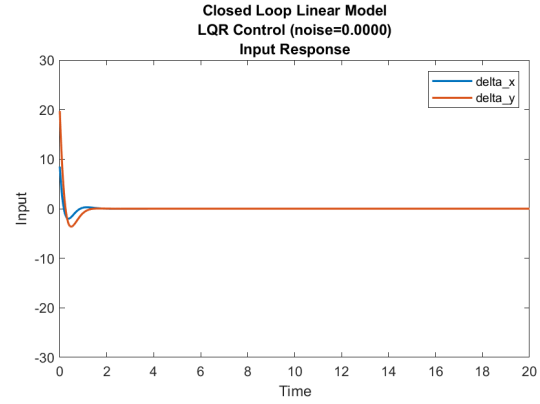


Fig. 23. Input response of closed loop linear system with LQR controller and no noise

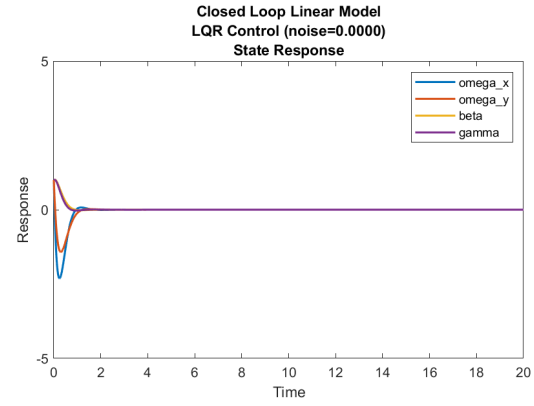


Fig. 24. State response of closed loop linear system with LQR controller and no noise

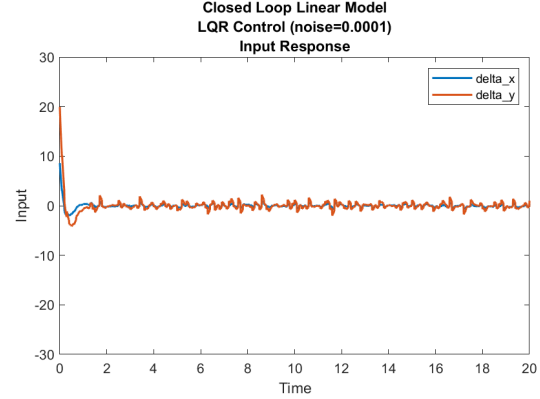


Fig. 25. Input response of closed loop nonlinear system with LQR controller and 0.0001 noise power

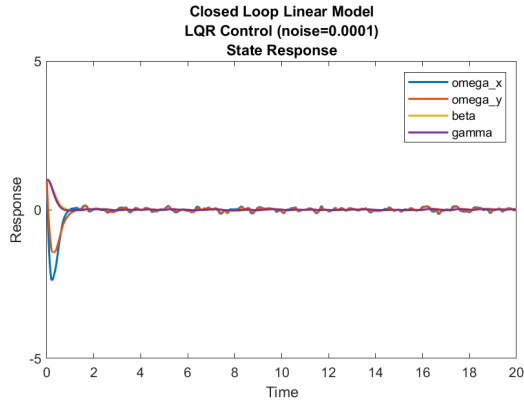


Fig. 26. State response of closed loop nonlinear system with LQR controller and 0.0001 noise power

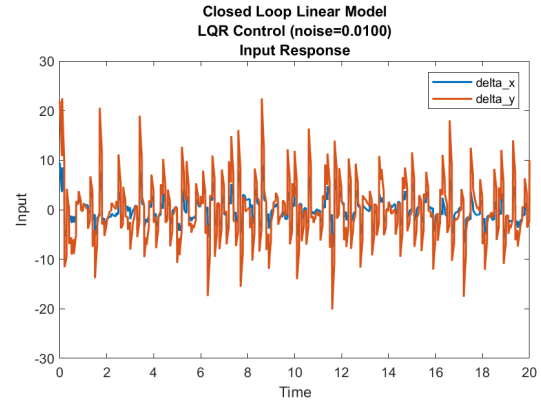


Fig. 29. Input response of closed loop nonlinear system with LQR controller and 0.01 noise power

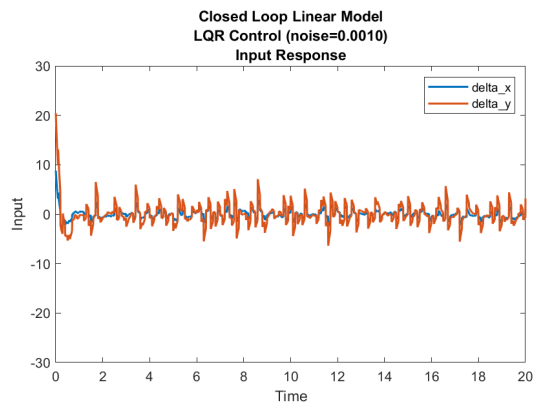


Fig. 27. Input response of closed loop nonlinear system with LQR controller and 0.001 noise power

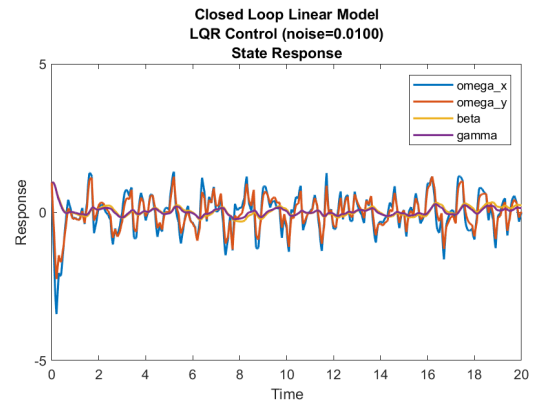


Fig. 30. State response of closed loop nonlinear system with LQR controller and 0.01 noise power

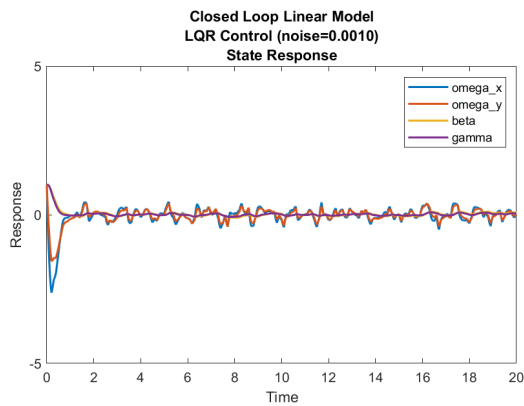


Fig. 28. State response of closed loop nonlinear system with LQR controller and 0.001 noise power

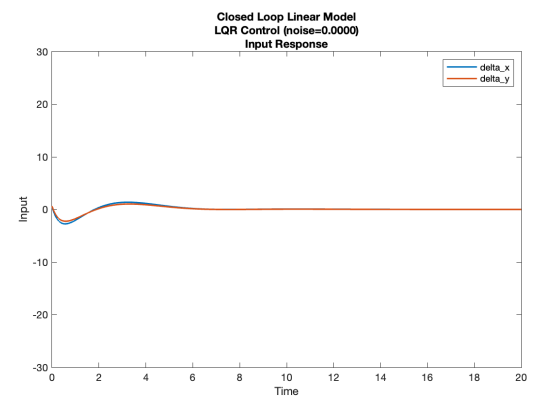


Fig. 31. Input response of closed loop linear system with Lyapunov test and no noise

It can be seen from Fig.23-30 that system with LQR controller is relatively sensitive to different levels of noise. The input reached 20 degrees under the influence of 0.01 noise power, and fluctuated violently.

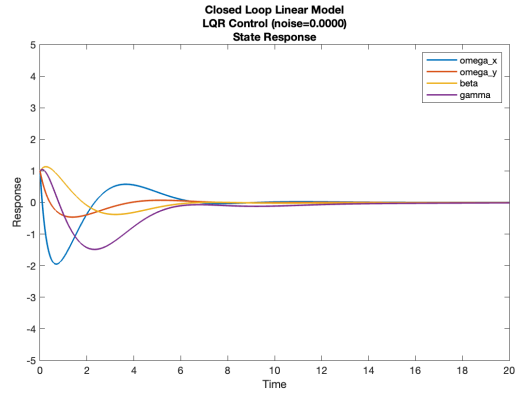


Fig. 32. State response of closed loop linear system with Lyapunov test and no noise

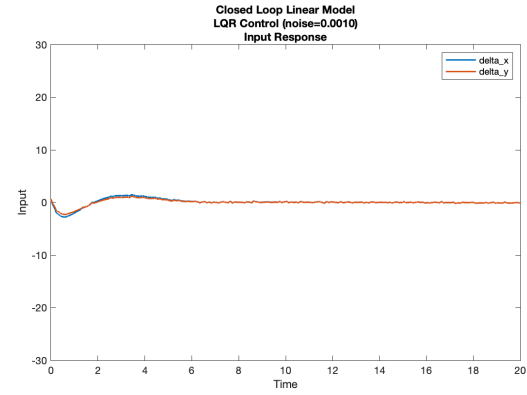


Fig. 35. Input response of closed loop linear system with Lyapunov test and 0.001 noise power

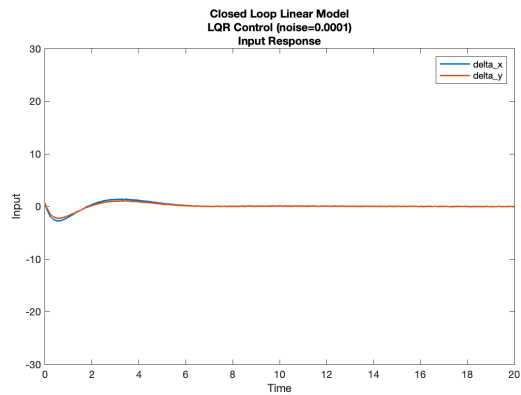


Fig. 33. Input response of closed loop linear system with Lyapunov test and 0.0001 noise power

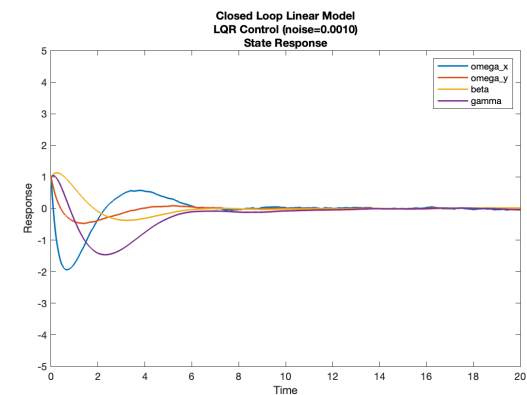


Fig. 36. State response of closed loop linear system with Lyapunov test and 0.001 noise power

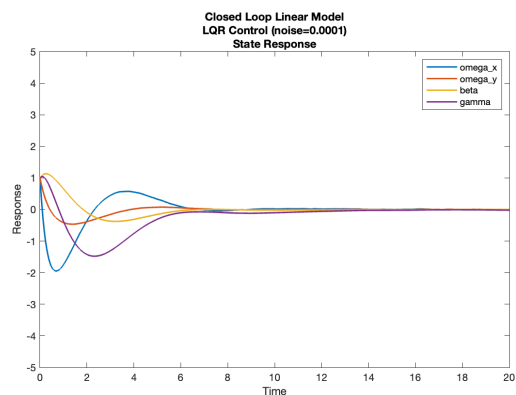


Fig. 34. State response of closed loop linear system with Lyapunov test and 0.0001 noise power

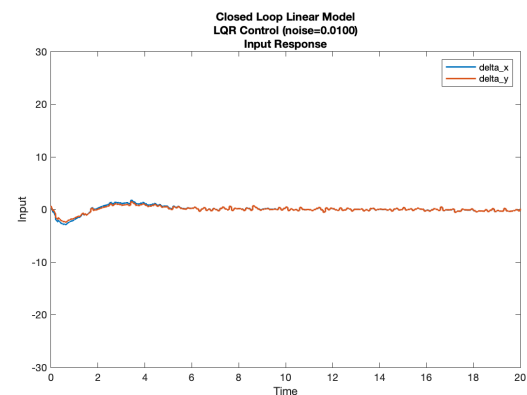


Fig. 37. Input response of closed loop linear system with Lyapunov test and 0.01 noise power

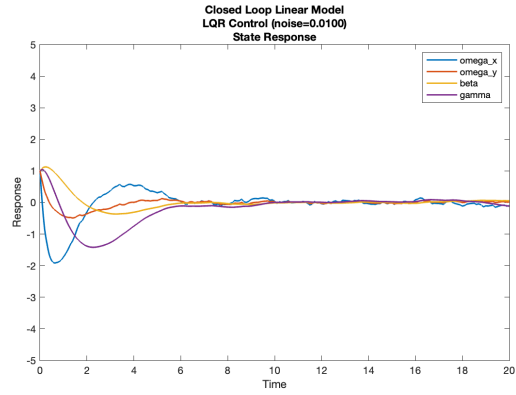


Fig. 38. State response of closed loop linear system with Lyapunov test and 0.01 noise power

It can be seen from fig.31-38 that the feedback controller based on Lyapunov test has a very good suppression effect on noise. Under the influence of noise power of 0.01, the status and input basically do not fluctuate much.

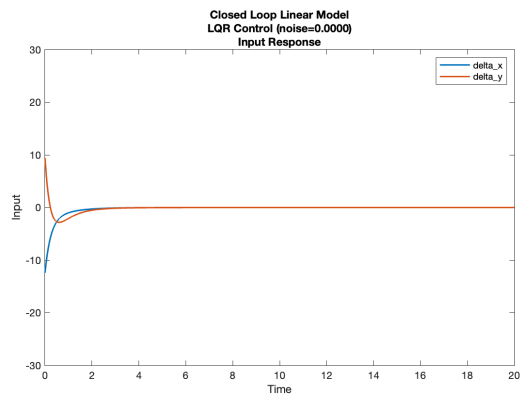


Fig. 39. Input response of closed loop linear system with eigenvalue assignment and no noise

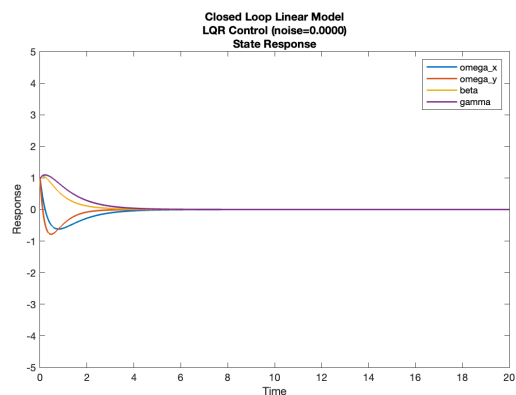


Fig. 40. State response of closed loop linear system with eigenvalue assignment and no noise

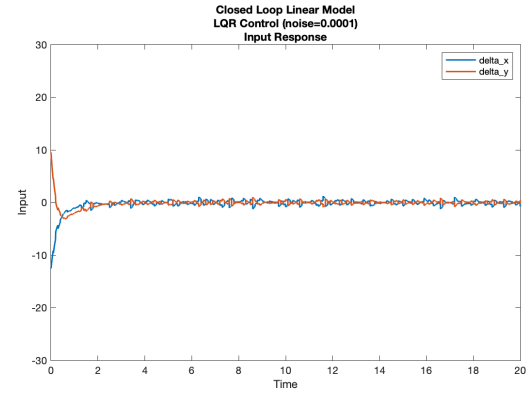


Fig. 41. Input response of closed loop linear system with eigenvalue assignment and 0.0001 noise power

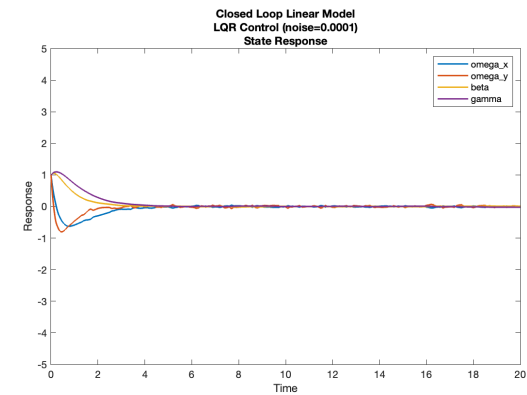


Fig. 42. State response of closed loop linear system with eigenvalue assignment and 0.0001 noise power

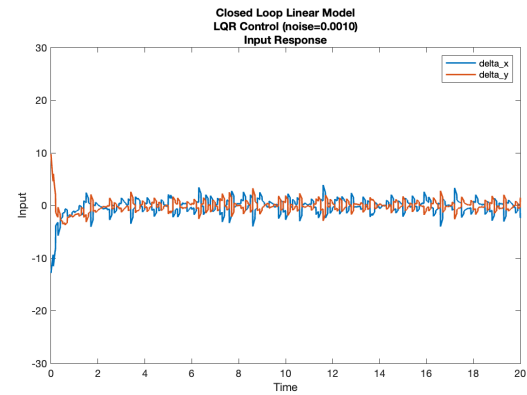


Fig. 43. Input response of closed loop linear system with eigenvalue assignment and 0.001 noise power

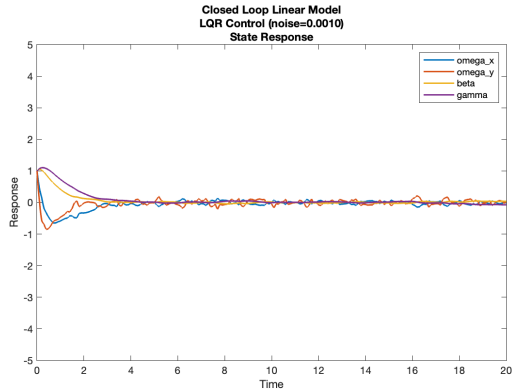


Fig. 44. State response of closed loop linear system with eigenvalue assignment and 0.001 noise power

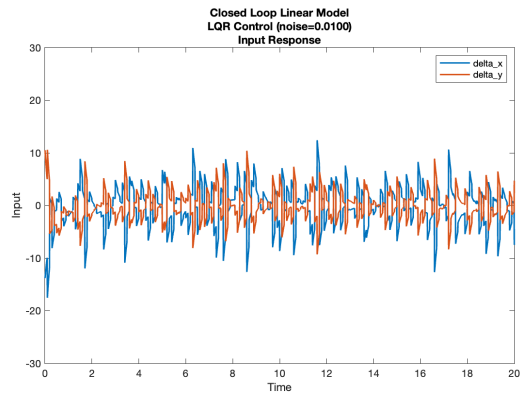


Fig. 45. Input response of closed loop linear system with eigenvalue assignment and 0.01 noise power

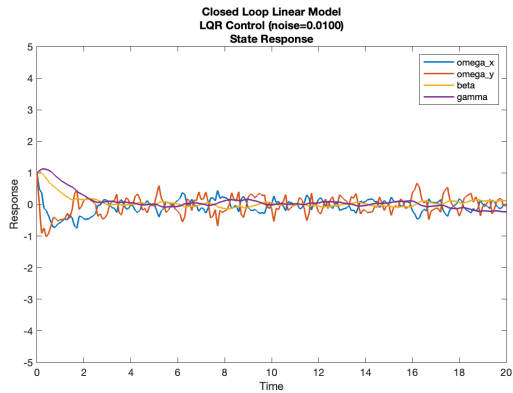


Fig. 46. State response of closed loop linear system with eigenvalue assignment and 0.01 noise power

It can be seen from fig.39-46 that the controller based on Eigenvalue assignment is still affected by noise to a certain extent, but the impact is not as severe as the LQR controller. Under the influence of 0.01power noise, the maximum value of the disturbed input reaches about 11 degrees.

Generally speaking, in terms of the noise suppression capabilities of the three control methods presented in this project, the feedback controller based on Lyapunov test has the best noise suppression effect, followed by the controller based on Eigenvalue assignment, and the LQR controller has the best effect on noise suppression. The inhibitory effect is the worst. However, due to the different debugging methods of the three controllers, there may be no reference value in comparing them with each other.

VI. HANDOUT 4

A. Handout 4 - Question 2.1

The observability matrix of our system is:

$$O = \begin{bmatrix} 1 & 0 & 0 & 0 \\ 0 & 1 & 0 & 0 \\ 0 & 0 & 1 & 0 \\ 0 & 0 & 0 & 1 \\ -1.8600 & -0.6600 & -8.8000 & 0 \\ -0.0200 & -0.2000 & -3.0000 & 0 \\ 0.2618 & 0.9991 & -0.0600 & 0.0280 \\ 1 & -0.0034 & 0 & 0 \\ 1.1690 & -7.4326 & 18.8765 & -0.2464 \\ -0.7442 & -2.9442 & 0.9561 & -0.0840 \\ -0.4947 & -0.4327 & -5.2976 & -0.0017 \\ -1.8599 & -0.6593 & -8.7899 & 0 \\ 2.6697 & 19.5757 & 10.8773 & 0.5285 \\ 1.6094 & 2.0356 & 15.3241 & 0.0268 \\ -0.4599 & -4.8799 & 5.9690 & -0.1483 \\ 1.1715 & -7.4227 & 18.8733 & -0.2461 \end{bmatrix}$$

The rank of the observability matrix is 4, which is full rank, so the system is observable.

B. Handout 4 - Question 2.2

Since our system is observable, we don't need to calculate the Kalman decomposition and our system is detectable.

C. Handout 4 - Question 2.3

This system is observable no matter which sensor fails, and it is also observable no matter which sensor work. This system will only be not observable when all sensor fails.

D. Handout 4 - Question 2.4

Since in our system, the number of states equals to the number of output. In the observer design, the second and the last output, which are ω_y as well as γ , are deleted. Fig. 47 and 48 are the states response for the linear system with and without observer. Fig. 49 and Fig. 50 are the states response for the nonlinear system with and without observer. It can be seen from the figure that the designed observer performs very well in tracking system states. The system response results predicted by the Observer are basically in line with the response curve of the original system.

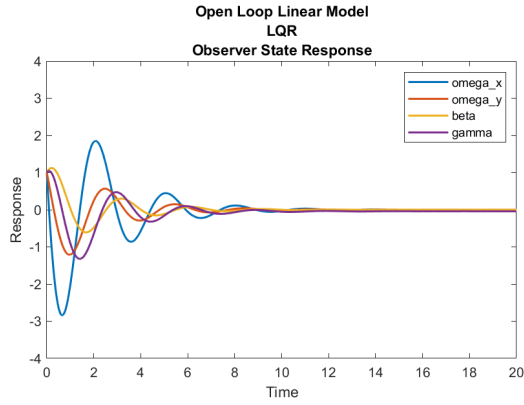


Fig. 47. States response for the linear system from observer

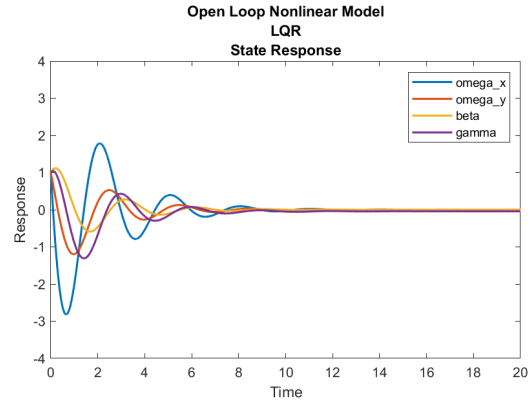


Fig. 50. States response for the nonlinear system

E. Handout 4 - Question 2.5

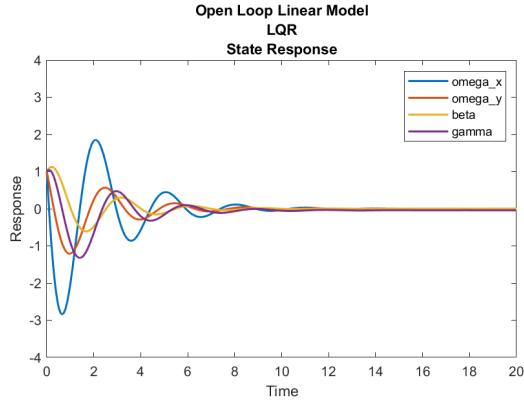


Fig. 48. States response for the linear system

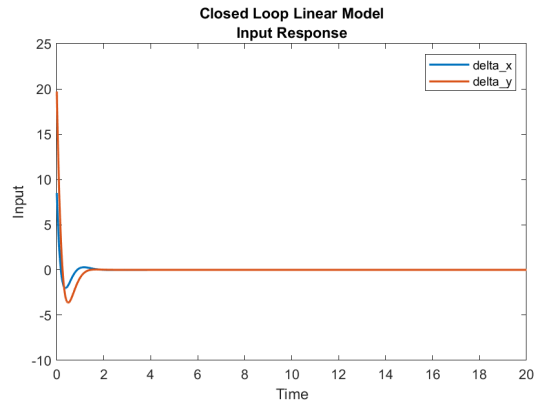


Fig. 51. Input response for the linear system with output feedback controller from observer

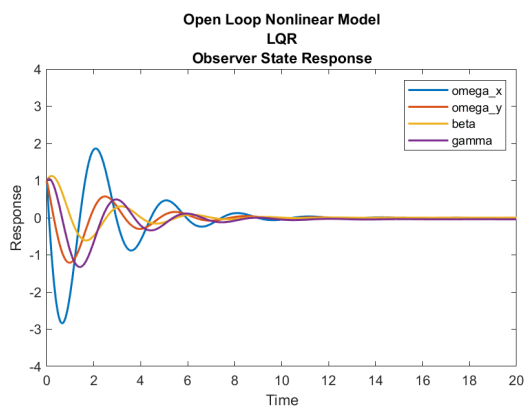


Fig. 49. States response for the nonlinear system from observer

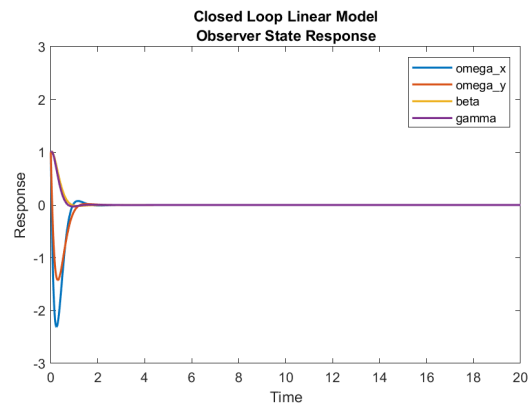


Fig. 52. Observer states response for the linear system with output feedback controller from observer

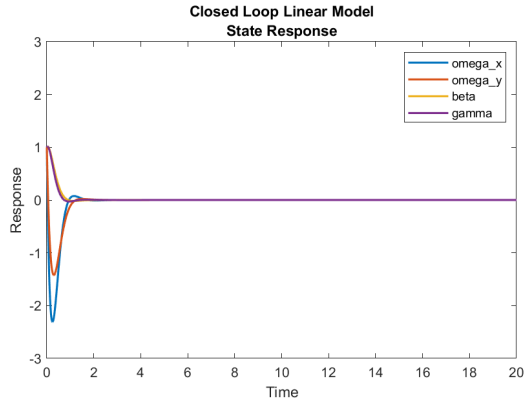


Fig. 53. States response for the linear system with output feedback controller from observer

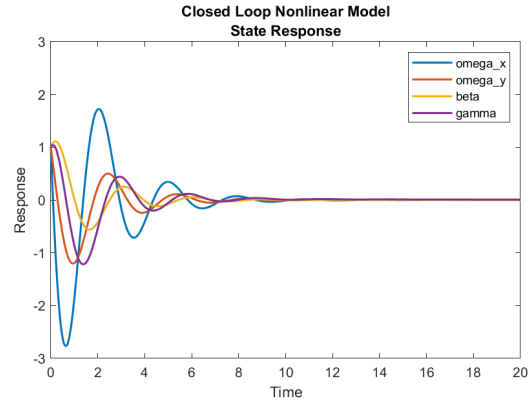


Fig. 56. States response for the nonlinear system with output feedback controller from observer

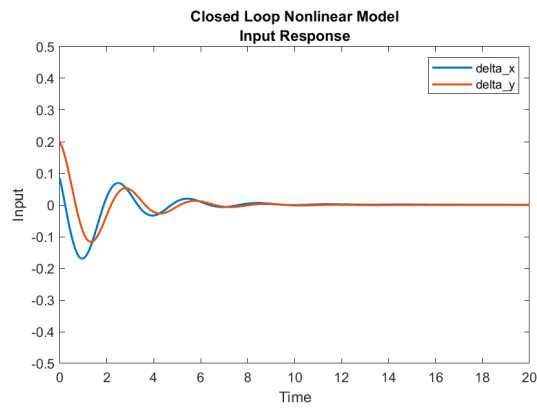


Fig. 54. Input response for the nonlinear system with output feedback controller from observer

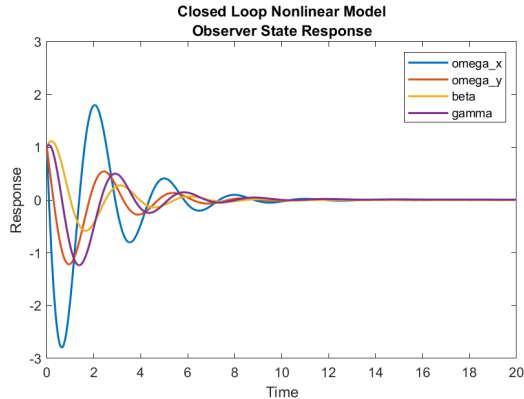


Fig. 55. Observer states response for the nonlinear system with output feedback controller from observer

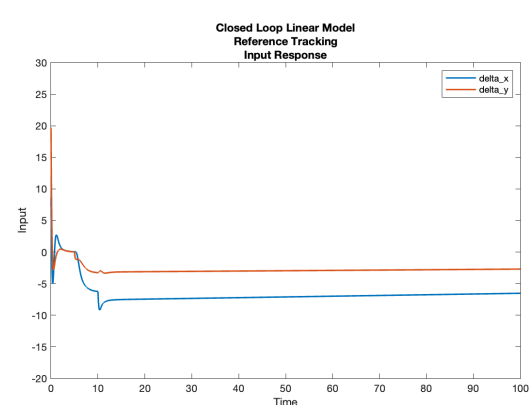


Fig. 57. Input response for the tracking linear system

It can be seen from fig. 51-56 that for linear systems and nonlinear systems, after using the feedback controller designed using the state predicted by the observer, under the same initial conditions, the input response curves and state response curves of the two systems are completely different. This is because the observer uses linear equations to predict the states, which will cause the state value predicted by the observer to be not much different from the state of the linear system itself, but there will be an error between the state of the nonlinear system, which will lead to two curves difference.

F. Handout 4 - Question 2.6

By setting ω and β as step reference signals, the tracking performance of the system was tested. The values of the two step signals are 2 degrees/s and 1 degree respectively, which are within a reasonable range. The input, observer, output and state response diagram of the linear system are shown in fig. 57-60, and the response of the nonlinear system are shown in fig. 61-64.

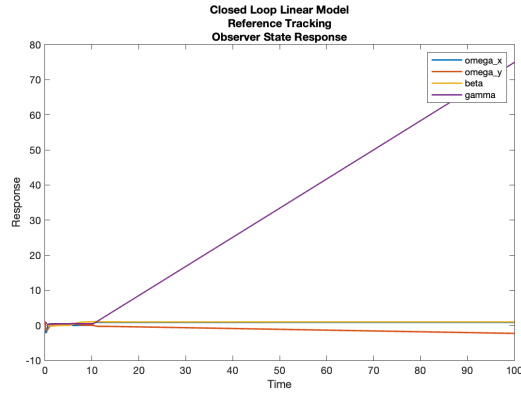


Fig. 58. States response from observer for the tracking linear system

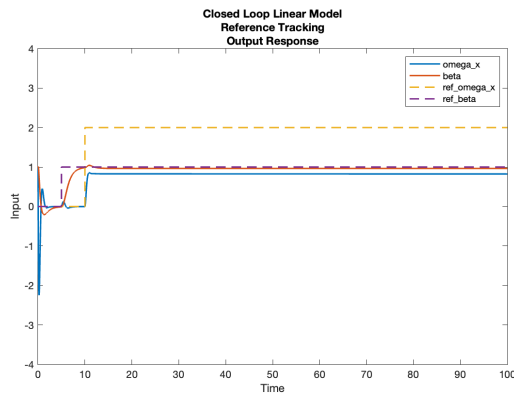


Fig. 59. Output response for the tracking linear system

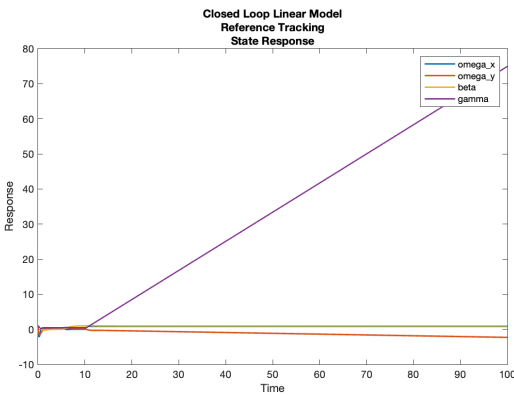


Fig. 60. States response for the tracking linear system

As shown in fig. 59, the tracking system demonstrates a good performance on tracking the beta signal, but it fails to track the ω_x signal. The value for ω_x converged at about 1 degree/s, which also causes the instability in the γ signal, leading to the Dutch Roll motion again. This can be attributed to the coupling in the lateral motion and roll motion. To keep the system in a stable flying condition, even though the Dutch Roll motion is sometimes acceptable, there is still a limit in the rolling

velocity since it also appears in the ω_y equation, and the lateral instability is more severe than the rolling instability. The input, observer, output and state response of the nonlinear system is shown in fig. 61-61.

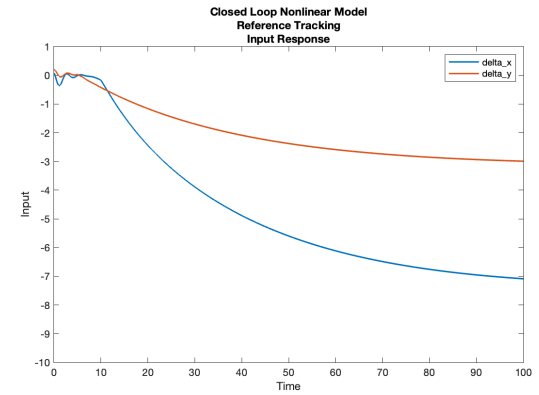


Fig. 61. Input response for the tracking nonlinear system

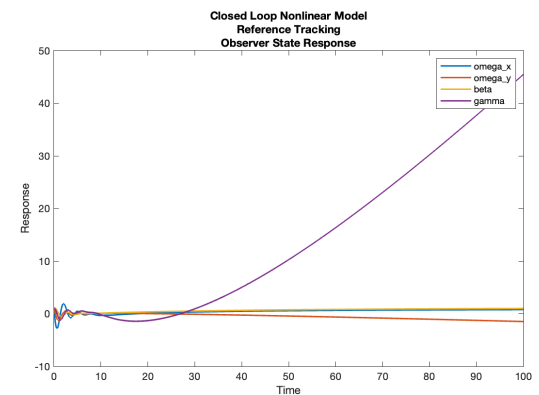


Fig. 62. States response from observer for the tracking nonlinear system

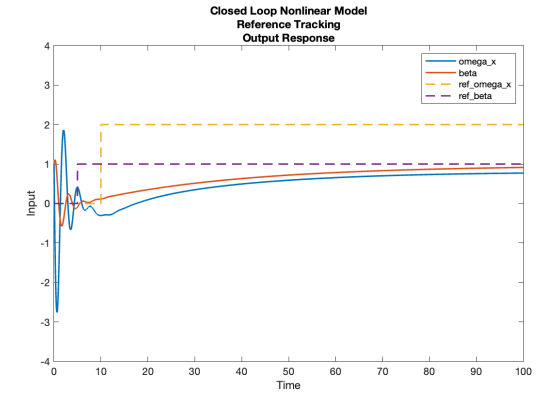


Fig. 63. Output response for the tracking nonlinear system

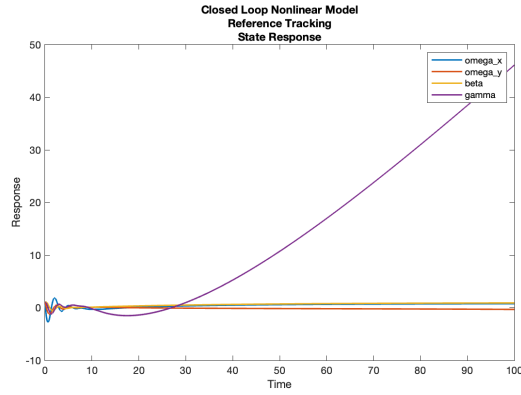


Fig. 64. States response for the tracking nonlinear system

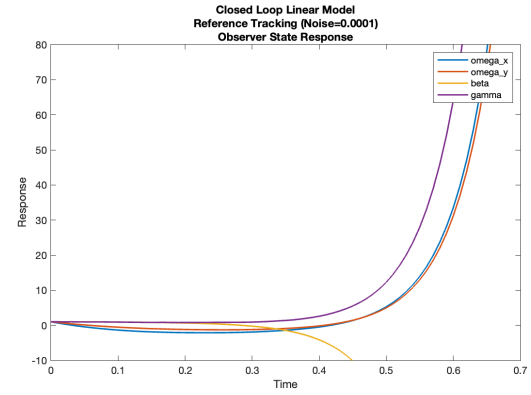


Fig. 66. States response from observer for the linear system with noise

As can be seen from fig.63, the two states are still one where tracking is successful and the other state is tracking failure. The difference is that the convergence speed of the two states is significantly slower. The source of this difference should be the assumptions made when the nonlinear system transforms into a linear system.

G. Handout 4 - Question 2.7

The input, observer, output and state response diagram of the linear system with noise in observer are shown in fig. 65-68, and the response of the nonlinear system with noise in observer are shown in fig. 69-72.

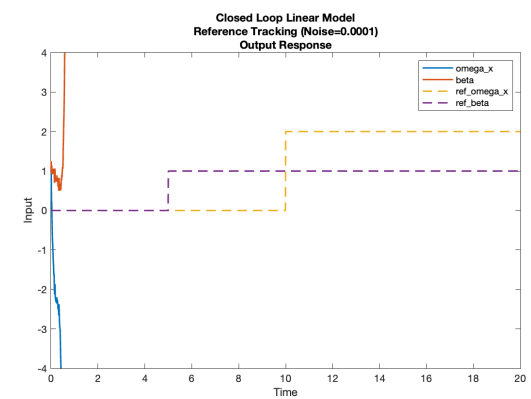


Fig. 67. Output response for the linear system with noise

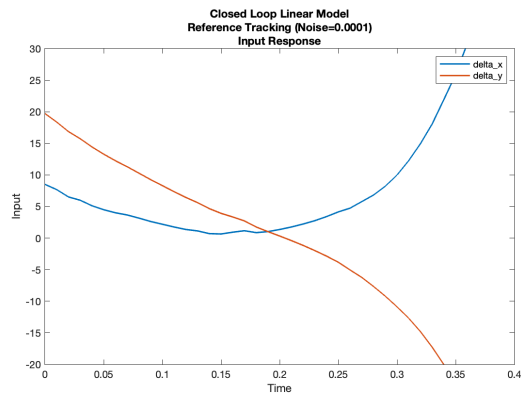


Fig. 65. Input response for the tracking linear system with noise

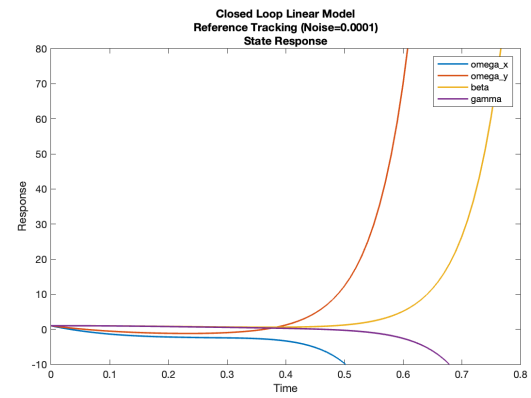


Fig. 68. States response for the nonlinear system with noise

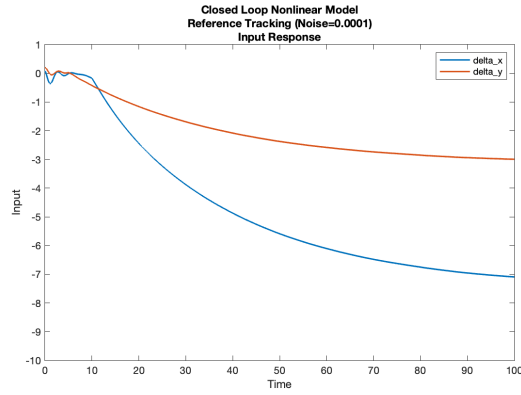


Fig. 69. Input response for the nonlinear system with noise

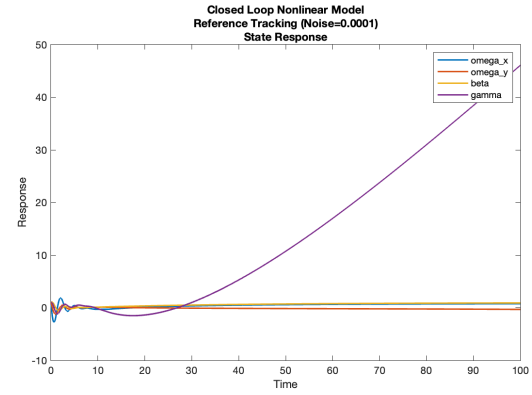


Fig. 72. States response for the nonlinear system with noise

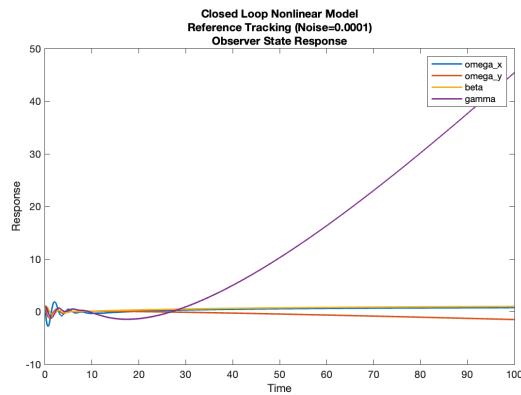


Fig. 70. States response from the observer for the nonlinear system with noise

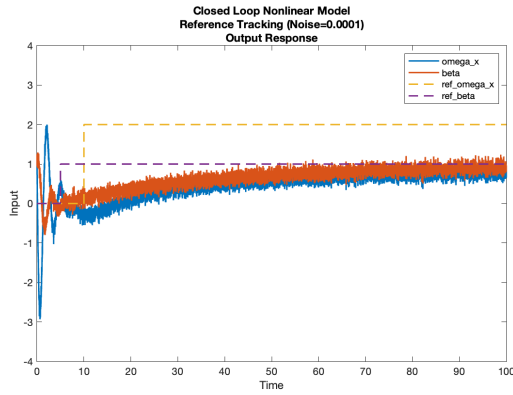


Fig. 71. Output response for the nonlinear system with noise

It can be seen from the figures that after adding noise to the observer of the linear system, all inputs and all states of the system become unable to converge, while the nonlinear system still shows a trend similar to the previous section, which shows that the nonlinear system's ability to resist noise interference is significantly stronger than that of a linear system. The approximation used in the derivation process will reduce the system's ability to resist interference.

REFERENCES

- [1] G. Li and Q. Fang, *Flight Dynamics of Winged Vehicles*, (in Chinese). China: Northwestern Polytechnical University Press, 2005. [Online]. Available: <https://bit.ly/4919oeF>
- [2] Q. Fang, Z. Zhu, and C. Sun, *Flight Dynamics and Guidance of Aircraft*, (in Chinese). China: Northwestern Polytechnical University Press, 2021. [Online]. Available: <https://bit.ly/3Mh3IDj>
- [3] Wikipedia, “MiG-25,” Available at https://en.wikipedia.org/wiki/Mikoyan-Gurevich_MiG-25 (2023/11/27).
- [4] ———, “J-20,” Available at https://en.wikipedia.org/wiki/Chengdu_J-20 (2023/11/27).
- [5] B. Carlson, A. H. Ullah, and J. Estevadeordal, “Experimental investigation of vortex-tube streamwise-vorticity characteristics and interaction effects with a finite-aspect-ratio wing,” *Fluids*, vol. 5, no. 3, p. 122, 2020. [Online]. Available: <https://doi.org/10.3390/fluids5030122>
- [6] D. Systems, “Mim-104.” Available at <http://www.designation-systems.net/dusrm/m-104.html> (2023/11/27).
- [7] Wikipedia, “Mim-104,” Available at https://en.wikipedia.org/wiki/MIM-104_Patriot (2023/11/27).

APPENDIX

A. Parameters

TABLE I
DEFINITION OF THE PARAMETERS

Parameter	Definition
g	gravity
v	velocity
r	radius
l	length
m	mass
P	thrust
Y	lift
Z	lateral force
α	attack angle
θ	angle of ballistic inclination
ϑ	pitch angle
β	sideslip angle
$\dot{\beta}$	change rate of β
ψ	yaw angle
γ	roll angle
γ_v	roll angle of speed
ψ_v	angle of ballistic deflection
ω_x	rotational angular velocity along the x-axis
ω_y	rotational angular velocity along the y-axis
ω_z	rotational angular velocity along the z-axis
δ_x	rudder deflection angle along the x-axis
δ_y	rudder deflection angle along the y-axis
Z^{δ_y}	partial derivative of Z to δ_y
Z^β	partial derivative of Z to β
J_x	moment of inertia along the x-axis
J_y	moment of inertia along the y-axis
J_z	moment of inertia along the z-axis
M_x	roll moment
M_y	yaw moment

Parameter	Definition
$M_x^{\omega_x}$	partial derivative of M_x to ω_x
$M_x^{\omega_y}$	partial derivative of M_x to ω_y
M_x^β	partial derivative of M_x to β
$M_x^{\delta_x}$	partial derivative of M_x to δ_x
$M_x^{\delta_y}$	partial derivative of M_x to δ_y
$M_y^{\omega_x}$	partial derivative of M_y to ω_x
$M_y^{\omega_y}$	partial derivative of M_y to ω_y
M_y^β	partial derivative of M_y to β
$M_y^{\dot{\beta}}$	partial derivative of M_y to $\dot{\beta}$
$M_y^{\delta_y}$	partial derivative of M_y to δ_y

TABLE II
VALUE OF THE PARAMETERS AT EQUILIBRIUM POINT

Parameter	Realistic Value	Unit
g	9.81	m/s
v	350.3552	m/s
r	0.1275	m
l	5.31	m
m	320	kg
P	20000	N
α	0.2618	$^\circ$
θ	-0.0688	$^\circ$
ϑ	0.1930	$^\circ$
Z^{δ_y}	-2018.0457	N
Z^β	13273.1810	N
J_x	2.601	$kg \cdot m^2$
J_y	751.8960	$kg \cdot m^2$
$M_x^{\omega_x}$	-4.8379	$kg \cdot m/s$
$M_x^{\omega_y}$	-1.7167	$kg \cdot m/s$
M_x^β	-22.8888	$kg \cdot m/s$
$M_x^{\delta_x}$	-2.5490	$kg \cdot m/s$
$M_x^{\delta_y}$	-2.0288	$kg \cdot m/s$
$M_y^{\omega_x}$	-15.0379	$kg \cdot m/s$
$M_y^{\omega_y}$	-150.3792	$kg \cdot m/s$
M_y^β	-2255.6880	$kg \cdot m/s$
$M_y^{\dot{\beta}}$	0	$kg \cdot m/s$
$M_y^{\delta_y}$	-676.7064	$kg \cdot m/s$

TABLE III
DEFINITION OF THE PARAMETERS

Force Coefficient	Value	Representation
b_{11}	1.86	$-\frac{M_x^{\omega x}}{J_x}$
b_{12}	0.66	$-\frac{M_x^{\omega y}}{J_x}$
b_{14}	8.8	$-\frac{M_x^\beta}{J_x}$
b_{17}	0.78	$-\frac{M_x^{\delta y}}{J_x}$
b_{18}	0.98	$-\frac{M_x^{\delta x}}{J_x}$
b_{21}	0.02	$-\frac{M_y^{\omega x}}{J_y}$
b_{22}	0.2	$-\frac{M_y^{\omega y}}{J_y}$
b_{24}	3	$-\frac{M_y^\beta}{J_y}$
\dot{b}_{24}	0	$-\frac{M_y^\beta}{J_y}$
b_{27}	0.9	$-\frac{M_y^{\delta y}}{J_y}$
b_{32}	-1	$-\frac{\cos \theta}{\cos \vartheta}$
b_{34}	0.06	$\frac{P - Z^\beta}{mv}$
b_{35}	-0.028	$-\frac{g}{v} \cos \vartheta$
b_{37}	0.018	$-\frac{Z^{\delta y}}{mv}$
a_{33}	0	$-\frac{g}{v} \sin \theta$
b_{52}	$0.0012 \Rightarrow -0.0034$	$-\tan \vartheta$